Solution grown double heterostructure on a large hybrid halide perovskite crystal

Chathuranga Hettiarachchi[*†]

Muhammad Danang Birowosuto[‡]   Tien Hoa Nguyen[*†]

Riyas Ahmad[†]   Kantisara Pita[*]   Nripan Mathews[†]

Cuong Dang[*†‡§]

Supplementary Information

- Figure S1: Absorbance Spectra of Cl-Br mixed Halide crystals
- Table S1. The relationship between solution composition and crystal.
- Table S2. The estimation of single crystal compositions based on lattice constants.
- Figure S2: Surface morphology of the crystals after the growth process.
- Figure S3. Effect of surface rinsing.
- Figure S4. An image of a sample cross section with 20 min layer growth.
- Figure S5. Cross section SEM image and comparison between EDS spectra from substrate and layer for a sample with 20min growth time.
- Table S3. Comparison of elemental composition of layer and seed regions of 20-min grown sample.
- Figure S6. Cross section SEM image and EDS elemental maps/line profiles for different growth times.
- Figure S7. Indexed EBSD patten
- Figure S8. Time resolved photoluminescence (TRPL) data.
- Table S4. Double exponential fitting of TRPL data

[*]Centre for OptoElectronics and Biophotonics (COEB), School of Electrical and Electronic Engineering, The Photonics Institute (TPI), Nanyang Technological University, 50 Nanyang Avenue, 639798, Singapore

[†]Energy Research Institute @NTU (ERI@N), Nanyang Technological University, Research Techno Plaza, X-Frontier Block, Level 5, 50 Nanyang Drive 637553, Singapore

[‡]CINTRA - CNRS/NTU/Thales UMI 3288, 50 Nanyang Drive, 637553, Singapore

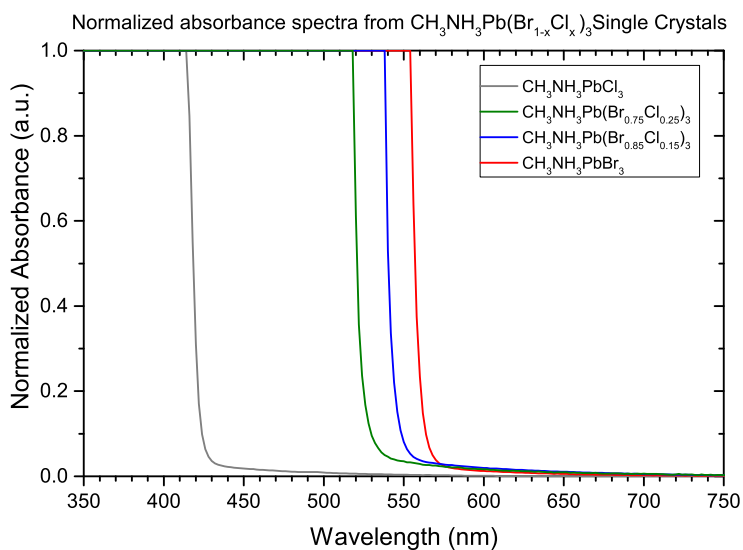[§]corresponding author HCDANG@ntu.edu.sg

Figure S1: Normalized absorbance spectra of crystals grown from the solutions with different halide compositions, gathered using transmission mode UV-Vis spectroscopy. Thickness of the crystal is in few millimetres; hence the transmission quickly becomes undetectable for photons with energy just higher than band gap (shorter wavelength).

Crystal Composition	Reaction	Cl/(Cl+Br)% in solution	Solvent	~Temperature (with 1mol dm^{-3} solution)
$CH_3NH_3PbBr_3$	$PbBr_2 + CH_3NH_3Br$	0%	DMF	80°C
$CH_3NH_3Pb(Br_{0.85}Cl_{0.15})_3$	$PbBr_2 + 0.75\ CH_3NH_3Br + 0.25\ CH_3NH_3Cl$	8.3%	DMF	75°C
$CH_3NH_3Pb(Br_{0.75}Cl_{0.25})_3$	$PbBr_2 + 0.50\ CH_3NH_3Br + 0.50\ CH_3NH_3Cl$	16.7%	DMF	65°C
$CH_3NH_3PbCl_3$	$PbCl_2 + CH_3NH_3Cl$	100%	DMF:DMSO 1:1 by vol	50°C

Table S1: The relationship between the composition of growth solution and crystal. Solution composition were adopted from Zhang et. al,[1]. Note that the crystal composition change from the solution composition due to differences in solubility.

Solution Composition	2nd Order angle 2θ (Degree)	Lattice Constant (Å)	Estimated Cl/(Cl+Br) ratio	Expected Cl/(Cl+Br) ratio	Crystal Composition
$CH_3NH_3PbBr_3$	30.11(3)	5.93(1)	0%	0%	$CH_3NH_3PbBr_3$
$CH_3NH_3PbBr_{2.75}Cl_{0.25}$	30.25(4)	5.90(2)	13(3)%	15%	$CH_3NH_3Pb(Br_{0.85}Cl_{0.15})_3$
$CH_3NH_3PbBr_{2.50}Cl_{0.50}$	30.41(4)	5.87(2)	25(3)%	25%	$CH_3NH_3Pb(Br_{0.75}Cl_{0.25})_3$
$CH_3NH_3PbCl_3$	31.43(4)	5.69(2)	100%	100%	$CH_3NH_3PbCl_3$

Table S2: The estimation of single crystal compositions based on lattice constants.

We determine the elemental composition using the Vegard's law, based on the lattice constants calculated from the second order (200) peak positions of PXRD spectrum. Vegard's law is an empirical rule, which assumes a linear relation between the composition ratio of a binary alloy and ratio between difference of lattice constants. If x is the Cl composition (i.e. $CH_3NH_3Pb(Br_{1-x}Cl_x)_3$), and we have experimental value for the lattice constant a_x, x can be estimated using the formula $x = (a_{Br} - a_x)/(a_{Br} - a_{Cl})$.

Spectrum	In stats.	C	N	Cl	Br	Pb
Layer	Yes	32.83	17.57	**1.07**	**36.94**	11.60
Substrate	Yes	29.51	21.48	**4.15**	**33.57**	11.29

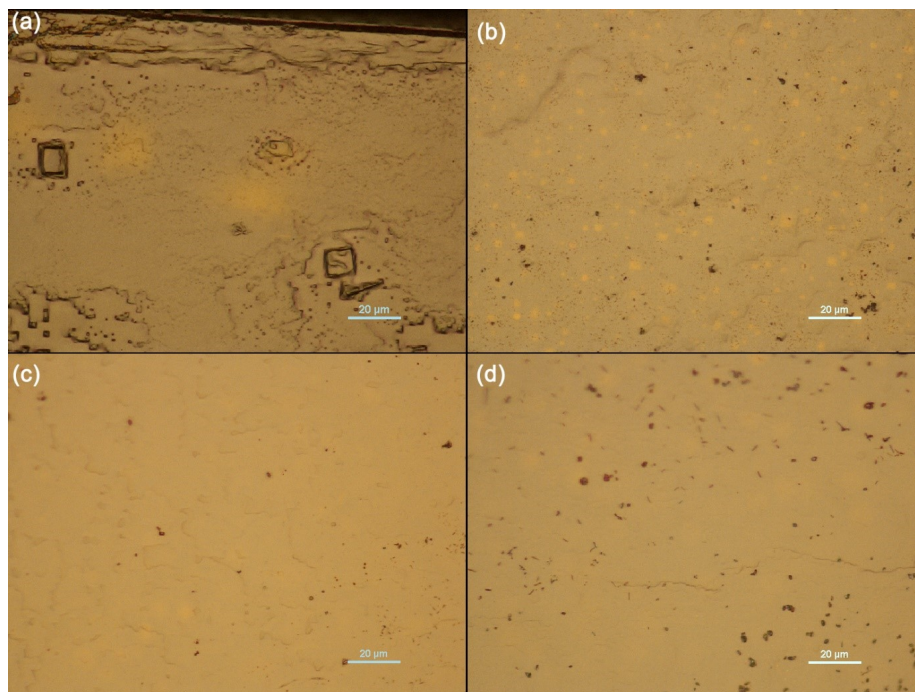Table S3: Comparison of elemental composition of layer and seed regions of 20 min grown sample.

Figure S2: Surface of the crystals. At **(a)** 0 min **(b)** 5 min **(c)** 10 min **(d)** 20 min growth time in 0.65M $CH_3NH_3PbBr_3$ solution at 75 °C.
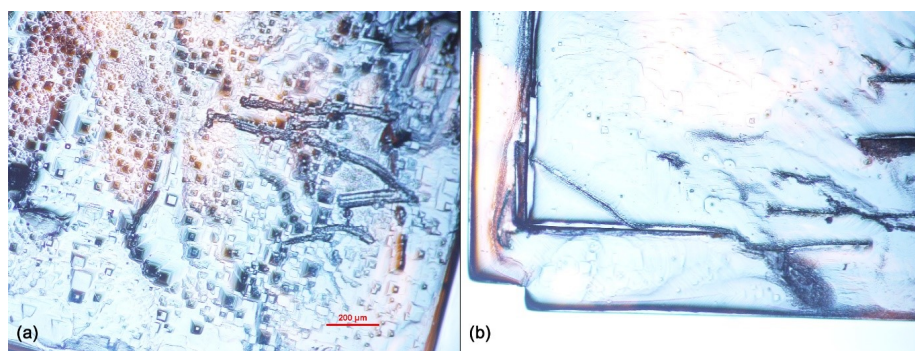

Figure S3: Effect of rinsing. Crystal surface unrinsed **(a)** and rinsed **(b)**. Rinsing is important to avoid secondary seed formation and mixing growth solution after extraction.

Figure S4: Stitched optical image of a sample cross section with 20 min layer growth.
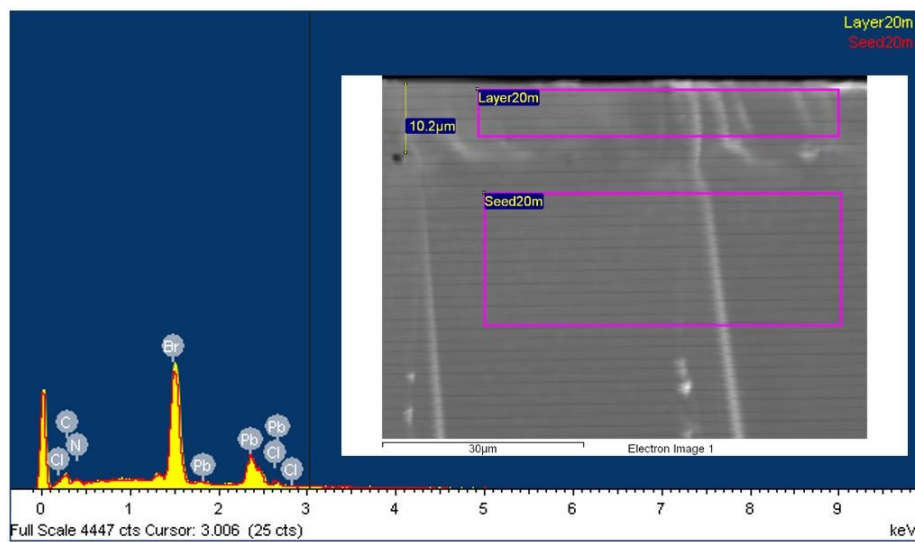

Figure S5: Comparison between EDS spectra from selected layer and seed regions of cross section from 20 min sample. Different between Br and Cl. Corresponding SEM image is inset. Processing option: All elements analyzed. All results in atomic%
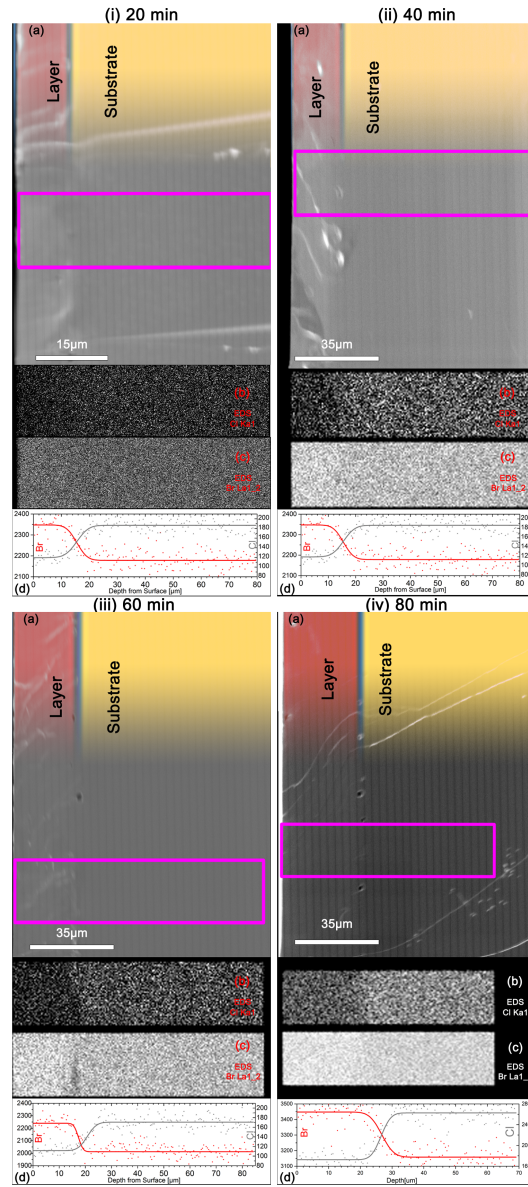
Figure S6: SEM image and elemental mapping of the cross section of hetero-structure with different growth time intervals from 5 min to 80 min (extended Figure 3). Layer growth solution concentration is 0.65 M and temperature maintained at 75 °C.

EDS Integrated elemental profile fitting for Br and Cl

Fick's second law (The diffusion equation)

$$\frac{\partial C}{\partial t} = D\frac{\partial^2 C}{\partial^2 x} \tag{1}$$

$InitialConditions$ $\qquad\qquad$ $BoundaryConditions$

$\qquad C(x,0) = C_1 \qquad x < 0 \qquad\qquad C(-\infty, t) = C_1$

$\qquad C(x,0) = C_2 \qquad x > 0 \qquad\qquad C(\infty, t) = C_2$

$\qquad$ Fitting function:

$$C(x,t) = c + d * erf(\frac{x-a}{b}) \tag{2}$$

a is the position of the interface, and b is diffusion length. c is the concentration measured at the interface, where the difference between interface and boundary concentrations is given by d. $erf(y) = \frac{2}{\pi}\int_0^y e^{-y^2} dy$ is the error function.

$\qquad$ Analytical solution:

$$C(x,t) = C_s + (C_2 - C_s) * erf(\frac{x-x_0}{2\sqrt{Dt}}) \tag{3}$$

$$C_s = (C_1 + C_2)/2 \quad , \quad a = x_0 \quad , \quad b = 2\sqrt{Dt}$$

Diffusion length can be stated in terms of diffusivity and time; however, further analysis is essential to determine the correct time parameters , since the layer is growing continuously.
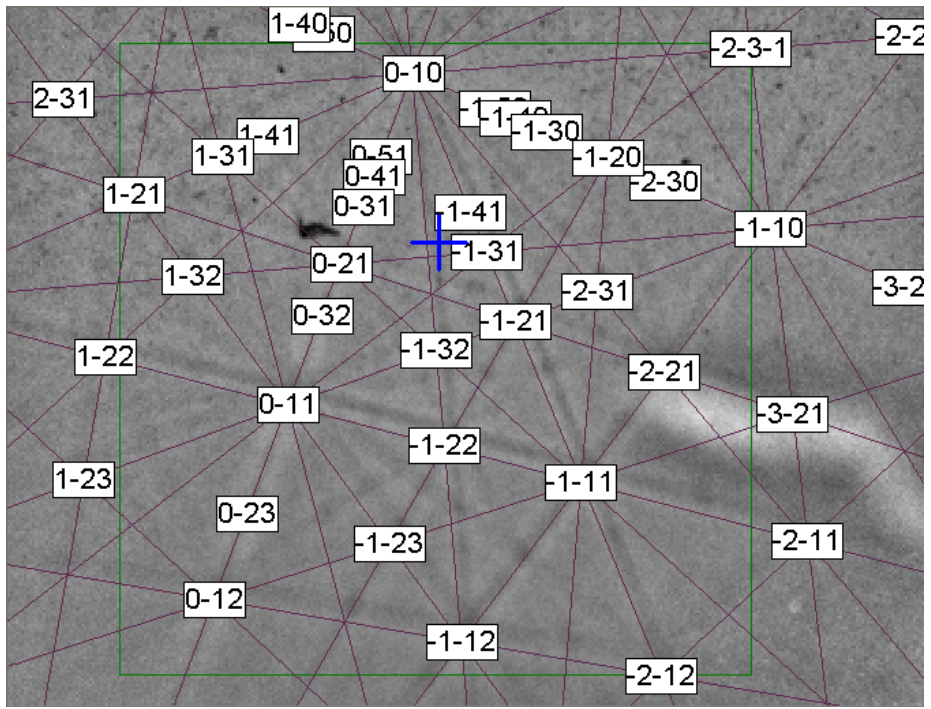
Figure S7: Indexed EBSD pattern. Pattern center is marked with the blue cross. The direct lattice indices (lattice vectors) of the zone axes are given at the high symmetry points
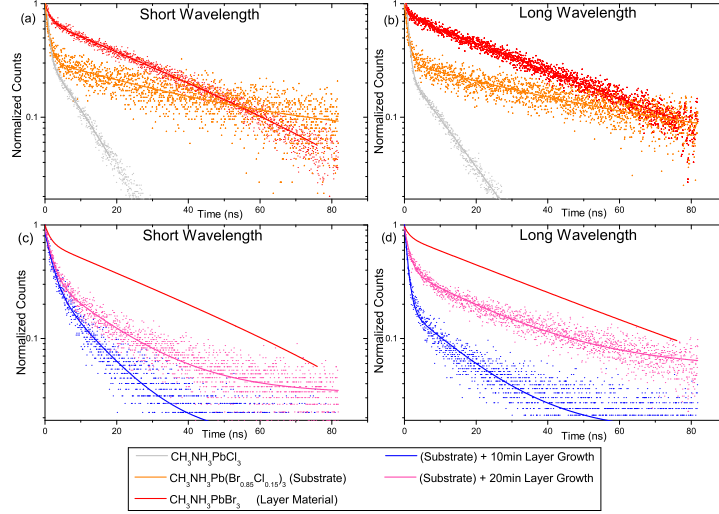
Carrier dynamics of the layers

Figure S8: Photoluminescence decay. **(a,b)** from crystal substrates and **(c,d)** layers at short wavelengths (peak wavelengths - 7.5 nm) and long wavelengths (peak wavelengths + 7.5 nm). Peak wavelengths are described in Table S4. The solid lines are the double exponential fits. The fits for $CH_3NH_3PbBr_3$ crystals are shown in **(c)** and **(d)** as comparison with the grown layers.

Time Resolved Photoluminescence(TRPL) measurements were performed to understand the quality of the overgrown layers. 371(5) nm 10 MHz pico second pulsed UV laser has been focused to the surface of the crystal though microscope objective (40 × , NA = 0.70). The micro-PL emission is confocal directed to a dispersion grating though a long pass filter appropriate to the peak wavelength (cut-off wavelength 400 nm for $CH_3NH_3PbCl_3$, and 450 nm for rest of the samples). For time-resolved PL measurements, the emission is directed to time correlated single photon counting card (TCSPC) though the dispersion grating configured at selected wavelengths below and above the peak position identified by PL measurements. 10 nm bandwidth resolution has been used to collect sufficient number of photons without overlapping the two measurement spectra. The instrument response function of the time-resolved system is 0.35 ns, which is appropriate for the measurements.

Double exponential decay function (Equation 4)has been used to fit the data in Origin Pro software. The data has been normalized to [0-1], and the original data has been shifted to offset the optical path delay such that the first data point have maximum value (i.e. 1). Then the double exponential decay function has been fitted with following formula.($t_0 = 0$). τ_1 and τ_2 are two lifetimes, and contributions of each component is calculated as area under the individual curve,

$I_1\tau_1$ and $I_2\tau_2$ for two components separately.

$$I = I_0 + I_1.e^{-\frac{(t-t_0)}{\tau_1}} + I_2.e^{-\frac{(t-t_0)}{\tau_2}} \tag{4}$$

Sample	Peak Wavelength (nm)	Lifetime at Short Wavelength (i.e. Peak -7.5 nm) (ns)		Lifetime at Long Wavelength (i.e. Peak +7.5 nm) (ns)	
		Fast	Slow	Fast	Slow
MAPbCl$_3$	405	0.7±0.1 (15%)	9.8±0.7 (85%)	0.7±0.1 (14%)	10.4±0.2 (86%)
MAPb(Br$_{0.85}$Cl$_{0.15}$)$_3$	519	1.1±0.1 (7%)	39.4±3.1 (93%)	1.0±0.1 (6%)	44.0±2.9 (94%)
MAPb(Br$_{0.85}$Cl$_{0.15}$)$_3$ / 10 min MAPbBr$_3$	524	2.0±0.1 (26%)	11.3±0.4 (74%)	0.9±0.1 (23%)	15.1±0.3 (77%)
MAPb(Br$_{0.85}$Cl$_{0.15}$)$_3$ / 20 min MAPbBr$_3$	539	1.9±0.1 (18%)	16.4±0.5 (82%)	1.4±0.1 (9%)	23.0±0.6 (91%)
MAPbBr$_3$	539	1.5±0.1 (2%)	33.5±0.6 (98%)	1.4±0.2 (1%)	34.7±0.7 (99%)

Table S4: Lifetime determined from the decay curves by fitting two exponential decay functions. The contribution has been calculated as the area under decay curve, for each component.

Studying carrier dynamics of the thin layer is helpful to understand its opto-electronic quality[2]. As an example, Time Resolved Photoluminescence (TRPL) is one of the methods to identify various recombination processes, such as intrinsic radiative recombination or various recombination mechanisms at defect states associated with the bulk or surface of the layer[3,4]. It is well known for perovskites to have different lifetime properties from bulk and surface regions[5–8]. In some cases, the energy bandgap difference between different origins can be low and the PL spectra can overlap each other by their broadband characteristics. However, the origins still can be characterized through TRPL as they may have different lifetimes.

Here we took two TRPL decay measurements filtered at two well separated wavelengths, namely short and long wavelengths with 10 nm resolution, see Methods section. We define the short and the long wavelengths as the peak wavelength minus and plus 7.5 nm, respectively. Before we measure hetero-structures, we first measure the TRPL of the pure crystals of $CH_3NH_3PbBr_3$ and $CH_3NH_3Pb(Br_{0.85}Cl_{0.15})_3$ as references to the layer samples as shown in Figures S8a and S8b. $CH_3NH_3PbCl_3$ TRPL data is also helpful to understand that the $CH_3NH_3Pb(Br_{0.85}Cl_{0.15})_3$ has an intermediate characteristic between its pure halide counterparts. For high quality crystals, there is no difference

between the short and the long wavelength emission. Hence, the emission could be from pure high quality crystal material, with homogeneously broaden line profile.

Among TRPL decay curves for three crystals studied in Figure S8a-b, the fastest decay curve is $CH_3NH_3PbCl_3$, while the curve of $CH_3NH_3Pb(Br_{0.85}Cl_{0.15})_3$ falls between $CH_3NH_3PbCl_3$ and $CH_3NH_3PbBr_3$. It is already known for a series of halide compounds, Chloride-Bromide-Iodide, with the same structure, the photoluminescence lifetime tends to be faster towards Chloride[9]. Thus, the emission lifetimes of pure crystals are good representation for the intrinsic emission in perovskite, since the crystals have limited extrinsic defects such as grain boundaries or interface defects. Then, the same characterization has been performed in layer samples for different growth times (Figure S8c-d). At shorter growth time, the decay characteristics deviate considerably from the substrate characteristics. With the increased growth time, it approaches to resemble the pure $CH_3NH_3PbBr_3$ emission characteristics.

To understand this behavior, considering the contribution from bulk and surface/ interface emissions is helpful. When the layer is thin, recombination mechanisms associated with defects at surface and interface have considerably high contribution on its rapid TRPL decay rate, with respect to the emission from bulk substrate or layer material[2]. This is evident from the drastic deviation of substrate emission decay behavior (Figure 3a-b) from the thin layer emission decay behavior (Figure S8c-d). At higher thicknesses, the sample gradually approach the layer material behavior which only consist of surface and bulk of $CH_3NH_3PbBr_3$ within the effective excitation and emission depth. However, it does not completely resemble the layer material decay characteristic, due to the contribution from propagating defects such as screw or edge dislocations originated at the layer growth interface.

Further in Figure S8c-d, it is evident in thick layer sample that the decay process is slower at longer wavelength than at the shorter wavelength. By fitting the decay curves with a double exponential decay function (Table S4), lifetime difference between short wavelength and long wavelength is clearly distinguishable, especially in slow decay component. This observation suggests that more localized low energy states exists in the layer layer. The lifetime of slow decay component gradually increases with the layer thickness at both short and long wavelengths. Also, contribution from fast component reduces with increasing layer thickness where it reaches just 1%-2% at the pure $CH_3NH_3PbBr_3$.

Hence, we think fast decay component is associated with interface defects, and probably non-radiative recombination. Graded band gap and mixed halide phases introduced by ion diffusion process are probably responsible for lifetime difference from short wavelength to long wavelength, due to carrier funneling toward low energy regions.

References

1 T. Zhang, M. Yang, E. E. Benson, Z. Li, J. van de Lagemaat, J. M. Luther, Y. Yan, K. Zhu and Y. Zhao, *Chem. Commun.*, 2015, **51**, 7820–7823.

2 Y. Wang, X. Sun, Z. Chen, Y.-Y. Sun, S. Zhang, T.-M. Lu, E. Wertz and J. Shi, *Advanced Materials*, 2017, **29**, 1702643.

3 G. Maculan, A. D. Sheikh, A. L. Abdelhady, M. I. Saidaminov, M. A. Haque, B. Murali, E. Alarousu, O. F. Mohammed, T. Wu and O. M. Bakr, *The Journal of Physical Chemistry Letters*, 2015, **6**, 3781–3786.

4 P. K. Nayak, D. T. Moore, B. Wenger, S. Nayak, A. A. Haghighirad, A. Fineberg, N. K. Noel, O. G. Reid, G. Rumbles, P. Kukura, K. A. Vincent and H. J. Snaith, *Nature Communications*, 2016, **7**, 13303.

5 D. Shi, V. Adinolfi, R. Comin, M. Yuan, E. Alarousu, A. Buin, Y. Chen, S. Hoogland, A. Rothenberger, K. Katsiev, Y. Losovyj, X. Zhang, P. A. Dowben, O. F. Mohammed, E. H. Sargent and O. M. Bakr, *Science*, 2015, **347**, 519–522.

6 K. J. Karki, M. Abdellah, W. Zhang and T. Pullerits, *APL Photonics*, 2016, **1**, 046103.

7 T. Yamada, Y. Yamada, H. Nishimura, Y. Nakaike, A. Wakamiya, Y. Murata and Y. Kanemitsu, *Advanced Electronic Materials*, 2016, **2**, 1500290.

8 H. Lu, H. Zhang, S. Yuan, J. Wang, Y. Zhan and L. Zheng, *Phys. Chem. Chem. Phys.*, 2017, **19**, 4516–4521.

9 M. D. Birowosuto and P. Dorenbos, *physica status solidi (a)*, 2009, **206**, 9–20.